White Rose Research Online

eprints@whiterose.ac.uk
https://eprints.whiterose.ac.uk
Universities of Leeds, Sheffield and York

Deposited via The University of Leeds.

White Rose Research Online URL for this paper:
https://eprints.whiterose.ac.uk/id/eprint/120552/

Version: Accepted Version

Article:
Watt, NT, Gage, MC, Patel, PA et al. (2017) Endothelial SHIP2 Suppresses Nox2 NADPH Oxidase–Dependent Vascular Oxidative Stress, Endothelial Dysfunction, and Systemic Insulin Resistance. Diabetes, 66 (11). pp. 2808-2821. ISSN: 0012-1797

https://doi.org/10.2337/db17-0062

© 2017 by the American Diabetes Association. This is an author produced version of a paper published in Diabetes. Uploaded in accordance with the publisher's self-archiving policy.

Reuse
Items deposited in White Rose Research Online are protected by copyright, with all rights reserved unless indicated otherwise. They may be downloaded and/or printed for private study, or other acts as permitted by national copyright laws. The publisher or other rights holders may allow further reproduction and re-use of the full text version. This is indicated by the licence information on the White Rose Research Online record for the item.

Takedown
If you consider content in White Rose Research Online to be in breach of UK law, please notify us by emailing eprints@whiterose.ac.uk including the URL of the record and the reason for the withdrawal request.

UNIVERSITY OF LEEDS
University of Sheffield
UNIVERSITY of York

Endothelial SHIP2 suppresses Nox2 NADPH oxidase-dependent vascular oxidative stress, endothelial dysfunction and systemic insulin resistance

*Nicole T Watt[1], *Matthew C Gage[1], Peysh A Patel[1], Hema Viswambharan[1], Piruthivi Sukumar[1], Stacey Galloway[1], Nadira Y Yuldasheva[1], Helen Imrie[1], Andrew MN Walker[1], Kathryn J Griffin[1], Natalia Makava[1], Anna Skromna[1], Katherine Bridge[1], David J Beech[1], Stéphane Schurmans[2], Stephen B Wheatcroft[1], Mark T Kearney[1], Richard M Cubbon[1]

[1]Leeds Institute of Cardiovascular and Metabolic Medicine, Leeds Multidisciplinary Cardiovascular Research Centre, University of Leeds, Leeds, LS2 9JT United Kingdom. [2] Laboratory of Functional Genetics, GIGA Research Centre, Université de Liège, Liège, Belgium. * Denotes joint first authors

Present address of Matthew Gage: Metabolism and Experimental Therapeutics, Faculty of Medical Sciences, University College London, London, United Kingdom.

Abbreviated title: Role of endothelial SHIP2

Address for Correspondence:

Professor Mark T Kearney[1]

E-mail: m.t.kearney@leeds.ac.uk

Tel: +441133437764

Word count: 4000

Figures: 8(+3) **Tables:** 0

Diabetes Publish Ahead of Print, published online August 22, 2017

Abstract

Shc homology 2-containing inositol 5´ phosphatase-2 (SHIP2) is as lipid phosphatase which inhibits insulin signaling downstream of phosphoinositide-3-kinase (PI3K); its role in vascular function is poorly understood. To examine its role in endothelial cell (EC) biology, we generated mice with catalytic inactivation of one SHIP2 allele selectively in EC (ECSHIP2$^{\Delta/+}$). Hyperinsulinemic euglycemic clamping studies revealed ECSHIP2$^{\Delta/+}$ were resistant to insulin-stimulated glucose uptake in adipose tissue and skeletal muscle, compared with littermate controls. EC from ECSHIP2$^{\Delta/+}$ had increased basal expression and activation of PI3K downstream targets, including Akt and endothelial nitric oxide synthase (eNOS), although incremental activation by insulin and shear stress was impaired. Insulin-mediated vasodilation was blunted in ECSHIP2$^{\Delta/+}$, as was aortic nitric oxide bioavailability. Acetylcholine-induced vasodilation was also impaired in ECSHIP2$^{\Delta/+}$, which was exaggerated in the presence of a superoxide dismutase/catalase mimetic. Superoxide abundance was elevated in ECSHIP2$^{\Delta/+}$ EC, and was suppressed by PI3K and Nox2 NADPH oxidase inhibitors. These findings were phenocopied in healthy human EC after SHIP2 silencing. Our data suggest that endothelial SHIP2 is required to maintain normal systemic glucose homeostasis and prevent oxidative stress-induced endothelial dysfunction.

Insulin resistance is a pathophysiological hallmark of obesity and type 2 diabetes mellitus (1). When systemic (2,3), or endothelium-restricted (4,5), insulin resistance leads to an unfavorable imbalance between endothelial cell (EC) generation of the signaling radical nitric oxide (NO) and potentially cytotoxic oxidants such as superoxide (4,5), and hydrogen peroxide (6). Whilst the effects of whole body and cell-specific insulin resistance on EC function are appreciated, the local and systemic consequences of increased insulin signaling in EC are less well characterized. To address this, we generated mice with endothelium-restricted inhibition of Shc homology 2-containing inositol 5´phosphatase 2 (SHIP2). SHIP2 is a lipid phosphatase which catalyzes the removal of the 5' phosphate group from phosphatidylinositol(3,4,5)-trisphosphate ($PI(3,4,5)P_3$) (7). $PI(3,4,5)P_3$ accumulation promotes the activity of signaling molecules, such as Akt; by reducing $PI(3,4,5)P_3$ accumulation, SHIP2 acts as a negative regulator of insulin-induced Akt signaling (7). Indeed, transgenic mice over-expressing SHIP2 have reduced insulin tolerance and blunted Akt activation in classic insulin target tissues (8).

Three different murine models of SHIP2 loss of function have been generated to examine the role of SHIP2 in insulin signaling. Clement *et al* described mice with deletion of *Inppl1* (which encodes SHIP2), although these had unplanned deletion of *Phox2a*, a transcription factor involved in normal development (9). Sleeman *et al* studied a second knockout mouse with deletion of *Inppl1*, but intact *Phox2a*; this also had developmental abnormalities (10). Recently, mice with catalytic inactivation of SHIP2 were generated by inserting Cre-recombinase-specific loxP sites into introns flanking *Inppl1* exons 18-19 (coding the SHIP2 catalytic domain) (11); these also had substantial developmental abnormalities making conclusions regarding insulin signaling challenging.

To improve our understanding of enhanced endothelial insulin signaling, whilst circumventing the developmental impact of global SHIP2 deletion, we generated mice in which the catalytically inactive SHIP2 described above (11) is restricted to EC using *Tie2-Cre* (referred to as ECSHIP2$^{\Delta/+}$). We hypothesized that endothelial SHIP2 activity is required to maintain appropriate systemic and vascular responses to insulin.

Research Design and Methods

Generating ECSHIP2$^{\Delta/+}$ mice. Mice were bred onto a C57BL/6J background for >10 generations in a conventional animal facility with 12-hour light/dark cycle. To examine the effect of chronically increased insulin signaling, male mice aged 10 months were used in all experiments, unless stated otherwise, conducted in accordance with accepted standards of humane animal care under UK Home Office project license 40/3523. A catalytically inactive SHIP2 mutant mouse was generated by inserting Cre recombinase-specific loxP sites into intronic regions flanking exons 18-19 of the *Inppl1* gene (11); mice with one floxed allele (SHIP2$^{(18\text{-}19)/+}$) were crossed with *Tie2*-Cre mice (Jackson Labs) to produce progeny with germline endothelium-specific SHIP2 inactivation (referred to as ECSHIP2$^{\Delta/+}$). Cre-positive SHIP2$^{+/+}$ littermates were controls in all experiments.

Metabolic tests. Glucose and insulin tolerance tests were performed by blood sampling after intraperitoneal (IP) injection of glucose (1mg/g) or recombinant human insulin (0.75unit/kg: Actrapid; Novo Nordisk) respectively, as described (4,5). Glucose concentrations were determined in whole blood by a portable meter (Roche). Plasma insulin concentrations were determined by enzyme-linked immunoassay (CrystalChem). Free fatty acids and triglycerides were measured in fasting plasma using colorimetric assays (Abcam) (12).

In vivo hyperinsulinaemic euglycaemic clamp studies. *In vivo* euglycaemic insulin clamps were performed at the Mouse Metabolic Phenotyping Centre at Vanderbilt University, as described (13). These use tracer techniques to assess: **1)** Whole body insulin sensitivity; **2)** Insulin suppression of endogenous (i.e. hepatic) glucose production; **3)** Rates of individual tissue glucose uptake.

Experimental protocol: Mice were maintained on a chow diet (Harlan Teklad Diet 7012). Catheters were implanted in a carotid artery for blood sampling, and jugular vein for infusions, 5 days before the study. On the morning of each study, food was removed and clamps initiated after a 5-h fast. 120 minutes (t=-120 min) prior to initiation of clamps, animals received a bolus (1.5μCi), followed by a continuous (0.075μCi/min) infusion of [3-^{3}H] glucose. Baseline blood or plasma parameters were determined in blood samples collected at −10 and 0min. At *t*=0 an insulin infusion (4mU/kg/min) was started, the [3-^{3}H]glucose infusion rate increased (0.15μCi/min), and a constant infusion of heparinized saline-washed with erythrocytes from donor animals (5.5μL/min) given to prevent a fall in hematocrit. These infusions were continued for the duration of the clamp (145min). Blood glucose was clamped at ~100-110mg/dL using variable glucose infusion rate (GIR). Blood glucose was monitored every 10 minutes to validate clamping, and GIR adjusted accordingly. Blood was taken between 80–120min for determination of [3-^{3}H]glucose. Clamp insulin was determined at *t*=120 and 145min. At 120min 13μCi 2[^{14}C]deoxyglucose ([^{14}C]2DG) was administered as an intravenous bolus. Blood was taken between 122–145min for determination of [^{14}C]2DG. After the last sample, mice were euthanized and tissues collected.

Plasma and muscle sample analysis: Immunoreactive insulin was assayed with rat radioimmunoassay kit (Millipore). To measure plasma 3-[^{3}H]-D-glucose, the sample was deproteinized with barium hydroxide ($Ba(OH)_2$) and zinc sulfate ($ZnSO_4$), dried, and

radioactivity determined using liquid scintillation counting. Excised soleus, gastrocnemius, superficial vastus lateralis and gonadal adipose tissue, were deproteinized with percholoric acid and then neutralizated to pH~7.5. A portion of the extract was counted ([2-^{14}C]DG and [2-^{14}C]DG-G-phosphate ([2-^{14}C]DGP) and a portion treated with $Ba(OH)_2$ and $ZnSO_4$ and the supernatant counted ([2-^{14}C]DG). Both [2-^{14}C]DG and [2-^{14}C]DG-G-phosphate ([2-^{14}C]DGP) radioactivity levels were determined using liquid scintillation counting.

Studies of vasomotor function in aortic rings. Vasomotor function was assessed *ex vivo* in aortic rings as described (2–5). Rings were mounted in an organ bath containing Krebs-Henseleit buffer (composition [in mmol/L]: NaCl 119, KCl 4.7, KH_2PO_4 1.18, $NaHCO_3$ 25, $MgSO_4$ 1.19, $CaCl_2$ 2.5, and glucose 11.0) and gassed with 95% O_2/5% CO_2. Rings were equilibrated at a resting tension of 3g for 45min. A cumulative dose response to the constrictor phenylephrine (PE) (1nmol/L to 10μmol/L) was performed. Vasodilation to insulin was assessed with incremental doses of actrapid insulin (0.1-1000mU/ml) in aortic segments pre-constricted maximally with PE. Relaxation responses to cumulative addition of acetylcholine (1nmol/L-10μmol/l) and sodium nitroprusside (0.1nmol/L-1μmol/l) were performed. The effects of MnTmPyP (10μmol/L for 30min, Calbiochem) on aortic relaxation were examined, as previously reported (2). Relaxation responses are expressed as % decrement in pre-constricted tension. Bioavailable NO in aortic segments subject to isometric tension was measured by recording the increase in tension elicited by L-NMMA (0.1mM) in aortic segments maximally pre-constricted with PE.

Amplex red assay for hydrogen peroxide in aorta. H_2O_2 was measured using an Amplex® Red Hydrogen Peroxide/Peroxidase Assay Kit (ThermoFisher), according to the manufacturer's protocol. Freshly harvested aortae were collected into modified Krebs-HEPES buffer, containing 20mM HEPES, 119mM NaCl, 4.6mM KCl, 1mM $MgSO_4.7H_2O$, 0.15mM

Na_2HPO_4, 0.4mM KH_2PO_4, 5mM $NaHCO_3$, 1.2mM $CaCl_2$ and 5.5mM glucose, pH 7.4. Aortas were cleaned of adipose tissue and divided into 2mm rings. Rings were incubated in 50µL of modified Krebs-HEPES buffer with half also receiving 1250U/mL catalase (free from tymol) for 1h at 37°C. 50µL freshly-prepared 100µM Amplex Red reagent with 0.2U/mL HRP was added to samples and incubated for 1 hour at 37°C, protected from light. Rings were removed from the samples and fluorescence measured on a VarioSkan (ThermoFisher) plate reader (excitation/emission 530/590nm). The mean reading with catalase was subtracted from the mean without catalase, and this value plotted on a simultaneously prepared H_2O_2 standard curve. Dry tissue mass was used for normalization (12).

Pulmonary endothelial cell isolation and culture. Primary endothelial cells were isolated from lungs by immunoselection with CD146-antibody-coated magnetic beads as reported (4,14) and cultured in 2ml EGM-2-MV (Lonza) supplemented with 5% fetal calf serum until confluent. These express a range of endothelial markers including eNOS, *Tie2* and CD102 protein (4,14).

SHIP2 activity assay. SHIP2 activity was measured using the 5'PtdIns(3,4,5)P_3 Phosphatase Activity Fluorescent Polarization Assay (Echelon Biosciences) according to the manufacturer's instructions, using a Polarstar Optima plate reader (BMG Labtech) with excitation at 550nm and measuring polarized emission at 580nm.

Nitric oxide synthase activity in endothelial cells. Active eNOS produces NO and L-citrulline from L-arginine in a stoichiometric reaction. Insulin-stimulated eNOS activity in EC was determined by conversion of [^{14}C]-L-arginine to [^{14}C]-L-citrulline as described (14,15). EC ($1x10^6$) were incubated at 37°C for 20 min in HEPES buffer pH 7.4 (in mmol/L): 10

HEPES, 145 NaCl, 5 KCl, 1 MgSO4, 10 glucose, 1.5 $CaCl_2$ containing 0.25% BSA. 0.5 μCi/ml [^{14}C]-L-arginine was then added for 5min prior to stimulation with insulin (100nmol/L) for 15min before the reaction was stopped with cold phosphate-buffered saline (PBS) containing 5mmol/L unlabeled L-arginine and 4mmol/L EDTA, after which cells were denatured in 95% ethanol. After evaporation, the pellet was dissolved in 20mmol/L HEPES-Na^+ (pH 5.5) and applied to a well-equilibrated DOWEX (Na^+ form) column. The eluate [^{14}C]-L-citrulline content was quantified by liquid scintillation and normalized against total protein mass.

Exposure of endothelial cells to flow-mediated shear stress. Pulmonary EC were seeded onto fibronectin-coated 6-well plates. Confluent monolayers were placed onto an orbital rotating platform (Grant Instruments) inside an incubator (16). The radius of orbit of the orbital shaker was 10mm and the rotation rate set to 210rpm for 10min, generating a shear force of 12 dyne/cm^2.

Lucigenin enhanced chemiluminescence. We used lucigenin (5μM), enhanced chemiluminescence to measure NAD(P)H-dependent superoxide production in pulmonary EC, as described (12). All experiments were performed in triplicate. Pulmonary EC were suspended in PBS containing 5% FCS, 0.5% BSA and 50uM gp91ds-tat (GenScript) or scrambled ds-tat peptide (GenScript) and incubated in 37˚C for 30min. Luminescence was measured upon addition of a non-redox cycling concentration of lucigenin (5μM) and NADPH (100μM), using an autodispenser (VarioSkan, ThermoFisher).

Cell lysis, immunoblotting, and immunoprecipitation. Pulmonary EC were lysed in extraction buffer containing (in mmol/L, unless otherwise specified) 50 HEPES, 120 NaCl, 1 $MgCl_2$, 1 $CaCl_2$, 10 NaP_2O_7, 20 NaF, 1 EDTA, 10% glycerol, 1% NP40, 2 sodium

orthovanadate, 0.5 μg/mL leupeptin, 0.2 phenylmethylsulfonyl fluoride, and 0.5 μg/mL aprotinin. Cell extracts were sonicated in an ice bath and centrifuged for 15 min, before protein measurement using the biocinochinic acid assay (ThermoFisher). Equal amounts of protein were resolved on SDS-polyacrylamide gels (ThermoFisher) and transferred to polyvinylidine difluoride membranes. Immunoblotting was carried out with primary antibodies produced by Cell Signaling Technologies, except for: mouse NOX2, mouse insulin receptor, mouse IRS1, mouse IRS2 and human SHIP2 (Abcam); human NOX2 and β-actin (Santa Cruz Biotechnology); mouse SHIP2 (Gift from Stéphane Schurmans, Université de Liège, Belgium). Blots were incubated with appropriate peroxidase-conjugated secondary antibodies and developed with enhanced chemiluminescence (Millipore).

Lentiviral knockdown of SHIP2 in human umbilical vein endothelial cells. Knockdown of SHIP2 in human umbilical vein endothelial cells (HUVEC; Promocell, UK) was performed with shRNA transduction using a lentivirus vector (Sigma-Aldrich SHCLNV-NM001567), as described (17). HUVEC were transduced with 10 MOI and incubated at 37ºC for 4 days prior to analysis. Control cells were transduced with GFP-targeting control shRNA lentivirus (Sigma-Aldrich SHC002H).

Gene expression. mRNA was isolated using TRIzol (ThermoFisher), and SHIP2 mRNA quantified using SYBR-Green based real-time quantitative PCR using (ABI Prism 7900HT, Applied Biosystems) (4). Primer details are as follows: truncated SHIP2 forward 5'-ACC-TTA-ACT-ACC-GCT-TAG-ACA-TGG-A; truncated SHIP2 reverse 5'-ATC-AGT-GCA-ACT-AAA-TCG-AAG-GAA; non-truncated region of SHIP2 forward 5'-AAG-ACT-ACT-CGG-CGG-AAC-CA; non-truncated region of SHIP2 reverse 5'- TGC-CGA-TCA-CCC-AAC-GA; β-actin forward 5'-CGT-GAA-AAG-ATG-ACC-CAG-ATC-A; β-actin reverse 5'-TGG-TAC-GAC-CAG-AGG-CAT-ACA-G. As published (12), RNA was also isolated from

purified $CD11b^+$ myeloid cells to define truncated SHIP2 expression. TaqMan (ThermoFisher) assays were used to measure expression of IL-1β (mm00434228_m1), IL-6 (mm00446190_m1) and TNFα (mm00443258_m1) in gastrocnemius muscle and epididymal adipose tissue.

Flow cytometry. Heparinised whole blood underwent erythrocyte lysis (Pharmalyse, BD Biosciences) prior to isolation of peripheral blood mononuclear cells (PBMC) by centrifugation. After blocking with CD16/32 Fc block (BD Biosciences), cells were stained anti-CD45-VioBlue, anti-CD11b-FITC, anti-Ly6G-PE (all Miltenyi Biotec) and Ly6C-APC (eBioscience). Paired samples were prepared with corresponding isotype-specific controls. Flow cytometry (LSRFortessa, BD Biosciences) was performed to define the following subsets: total leukocytes ($CD45^+$); myeloid cells ($CD45^+CD11b^+$); monocytes ($CD45^+CD11b^+Ly6G^-Ly6C^+$); neutrophils ($CD45^+CD11b^+Ly6G^{hi-}Ly6C^{hi}$); 'inflammatory' monocytes ($CD45^+CD11b^+Ly6G^-Ly6C^{hi}$); 'patrolling' monocytes ($CD45^+CD11b^+Ly6G^-Ly6C^{lo}$). All populations are expressed as cells/ml blood.

Cytokine ELISA. Serum IL-6 and TNFα were measured with commercially available ELISAs according to manufacturers' instructions (Abcam) (12).

Histology. 1) Adipose inflammation. Epididymal fat fixed in 4% paraformaldehyde was embedded in paraffin blocks and 5-micron sections stained with Sirius Red (Sigma) to demarcate collagen deposition, a feature of inflammation (18). Sirius red percentage area staining was calculated with Image J (NIH). **2) Adipose vascularity.** Epididymal fat fixed in 1% paraformaldehyde, then stained with lipidtox-green (ThermoFisher) and isolectin-B4-Alexa647 (ThermoFisher) was wholemounted in chamber slides and imaged with confocal microscopy (Zeiss LSM880). Vascular (Isolectin-B4) percentage area was calculated in

thresholded 4-micron maximum intensity projections using ImageJ (NIH). **3) Skeletal muscle vascularity.** Gastrocnemius muscle fixed in 4% paraformaldehyde was embedded in OCT (TissueTek, Sakura) and snap-frozen. 5-micron cryosections were stained with isolectin-B4-Alexa647 (ThermoFisher) and DAPI (Southern Biotech) then imaged with confocal microscopy (Zeiss LSM880). Vascular (Isolectin-B4) percentage area was calculated in thresholded 2-micron maximum intensity projections using ImageJ (NIH).

Statistics. Results are expressed as mean (SEM). Comparisons within groups were made using paired Student's *t*-tests and between groups using unpaired Student's *t*-tests or repeated-measures ANOVA, as appropriate. $P<0.05$ was considered statistically significant.

Results

Basic characterization of mice with endothelium-specific inactivation of SHIP2. To examine the effect of reducing the restraining role of SHIP2 on insulin action specifically in the endothelium, we generated mice with Tie2-Cre mediated catalytic inactivation of one SHIP2 allele (ECSHIP2$^{\Delta/+}$). ECSHIP2$^{\Delta/+}$ mice were born with the same frequency as control littermates. There was no difference in gross appearance (**Fig. 1A**), organ weight (**Fig. 1B**), or body length (**Fig. 1C**), when comparing ECSHIP2$^{\Delta/+}$ and control, although 10 month-old ECSHIP2$^{\Delta/+}$ mice were slightly heavier (**Fig. 1D**). We quantified truncated SHIP2 mRNA in organs with differing vascularity; as expected, SHIP2$^{\Delta 18\text{-}19}$ mRNA was only detectable above non-specific fluorescence in ECSHIP2$^{\Delta/+}$ organs, not control organs (**Fig. 1E**). SHIP2$^{\Delta 18\text{-}19}$ mRNA was also undetectable in non-endothelial cells from ECSHIP2$^{\Delta/+}$ lungs (**Fig. 1F**), but was just detectable in CD11b^{+} myeloid cells (>3000-fold lower than ECSHIP2$^{\Delta/+}$ PEC, and ≈5-fold above non-specific fluorescence **Sup. Fig. 1A**). Endothelial SHIP2 protein expression was mildly reduced in ECSHIP2$^{\Delta/+}$ mice (**Fig. 1G**), whilst SHIP2 activity was substantially

reduced (**Fig. 1H**), in keeping with targeted catalytic domain deletion, as shown previously in work using SHIP2$^{(18\text{-}19)/+}$ mice (11).

ECSHIP2$^{\Delta/+}$ mice do not exhibit a pro-inflammatory state. As very low-level expression of truncated SHIP2 was found in myeloid cells, we conducted a detailed assessment of systemic and tissue-specific inflammation. Flow cytometry revealed no difference in circulating leukocyte populations (**Sup. Fig. 1B**), and leukocyte SHIP2 activity was comparable in ECSHIP2$^{\Delta/+}$ and control littermates (**Sup. Fig. 1C**). ECSHIP2$^{\Delta/+}$ had normal serum TNFα and IL-6 (**Sup. Fig. 1D-E**), along with expression of TNFα, IL-1β, and IL-6 in white adipose tissue and skeletal muscle (**Sup. Fig. 1F**). We found no evidence of altered adipose tissue inflammation using Sirius Red collagen staining (**Sup. Fig. 1G**).

ECSHIP2$^{\Delta/+}$ mice have reduced glucose tolerance and insulin sensitivity. Compared to control littermates, ECSHIP2$^{\Delta/+}$ mice had higher fasting glucose (**Fig. 2A**), similar fasting insulin concentrations (**Fig. 2B**), and higher HOMA-IR (**Fig. 2C**). ECSHIP2$^{\Delta/+}$ had delayed normalization in capillary glucose during glucose tolerance testing (**Fig. 2D**), but insulin tolerance rests were similar to control littermates (**Fig. 2E**). Serum free fatty acids (**Fig. 2F**) and triglycerides (**Fig. 2G**) were not altered in ECSHIP2$^{\Delta/+}$. In hyperinsulinemic euglycemic clamp studies, ECSHIP2$^{\Delta/+}$ mice required approximately 25% less glucose to maintain euglycemia than controls (**Fig. 3A**). In tracer studies, glucose uptake into adipose tissue and skeletal muscle was reduced (**Fig. 3B**), whereas hepatic glucose output was no different between ECSHIP2$^{\Delta/+}$ and controls (**Figs. 3C,D**).

Endothelial cells from ECSHIP2$^{\Delta/+}$ mice have increased basal activation of signaling molecules downstream of PI3K, although incremental activation by insulin and shear stress is impaired. In the endothelium, PI3K transduces insulin signaling by catalyzing the

addition of a phosphate group to the 3'-position of inositol rings, generating 3'-phosphoinositides, including $PI(3,4,5)P_3$, which by activating phosphoinositide dependent kinase-1 (PDK1) activates the serine/threonine kinase Akt/PKB (19). Akt activates downstream signaling molecules including eNOS (20). ECSHIP2$^{\Delta/+}$ had increased basal expression of total PDK1 and pPDK1, total Akt and T308 pAkt, total eNOS and S1177 peNOS, Rictor (which phosphorylates Akt at S473) and pRictor (**Fig. 4A**). Importantly, 6-week old ECSHIP2$^{\Delta/+}$ mice had normal endothelial total Akt, Rictor and eNOS expression, and normal adipose tissue and skeletal muscle vascularity (**Sup. Fig. 2**), suggesting adulthood signaling abnormalities do not reflect persistent developmental abnormalities. ECSHIP2$^{\Delta/+}$ had comparable insulin-stimulated induction of Akt S473 phosphorylation, but diminished downstream induction of eNOS S1177 phosphorylation, compared to control (**Fig. 4B**). PI3K/Akt also mediate shear-induced eNOS activation in EC; ECSHIP2$^{\Delta/+}$ EC exhibited no increase in the phosphorylation of Akt S473 or eNOS S1177 in response to shear stress (**Fig. 4C**). Notably, we found no significant differences in basal or insulin-stimulated phosphorylation of the insulin receptor or insulin receptor substrates 1/2 (**Sup. Fig. 3**).

ECSHIP2$^{\Delta/+}$ mice have blunted acetylcholine- and insulin-mediated aortic vasodilatation associated with vascular oxidative stress. *Ex vivo* aortic vasomotor responses were studied in organ bath apparatus. Consistent with our findings in EC, ECSHIP2$^{\Delta/+}$ had blunted insulin-mediated vasodilation (**Fig. 5A**). ECSHIP2$^{\Delta/+}$ exhibited significantly less constriction to the non-selective NOS inhibitor L-NMMA (**Figs. 5B-D**), indicative of reduced NO biogenesis in response to isometric tension. There was subtle impairment of acetylcholine-induced relaxation in ECSHIP2$^{\Delta/+}$ (**Fig. 5E**), but SNP responses were comparable to control (**Fig. 5F**). To explore whether vasodilating oxidants were masking more substantial impairment of acetylcholine-mediated vasodilation in ECSHIP2$^{\Delta/+}$, we repeated acetylcholine relaxation studies in the presence of the superoxide dismutase/catalase mimetic MnTmPyP. MnTmPyP

reduced acetylcholine-mediated aortic relaxation in ECSHIP2$^{\Delta/+}$ and control vessels, but the extent of inhibition was significantly greater in ECSHIP2$^{\Delta/+}$ (**Figs. 5G-K**). Hydrogen peroxide, the more stable product of superoxide dismutation, was also elevated in ECSHIP2$^{\Delta/+}$ aortae (**Fig. 5L**). In isolated lung EC, superoxide abundance was increased, as assessed by lucigenin-enganced chemiluminescence and with dihydroethedium fluorescence (**Fig. 6A**). Superoxide is generated by many enzymes, and we have shown Nox2 NADPH oxidase is a critical pathophysiological source of superoxide in models of global insulin resistance (4,5). In ECSHIP2$^{\Delta/+}$ EC, Nox2 protein expression was increased (**Fig. 6B**). Moreover, superoxide abundance was normalized with the Nox2 specific inhibitor Gp91ds-tat (**Fig. 6C**), and the PI3K inhibitors Wortmannin and LY294002 (**Fig. 6D**). Oxidative stress is often associated with reduced eNOS activity, and this was confirmed in ECSHIP2$^{\Delta/+}$ EC treated with insulin (**Fig. 6E**).

SHIP2 knockdown in human EC phenocopies the signaling abnormalities of ECSHIP2$^{\Delta/+}$. Next, we sought to validate and generalize the mechanistic data from our murine model, using a complementary system in human endothelial cells. We used lentiviral vectors to express SHIP2-targeting shRNA, or a non-targeting control shRNA, to knockdown SHIP2 in HUVEC, achieving ≈75% reduction in SHIP2 protein, versus control (**Fig. 7A**). As seen in ECSHIP2$^{\Delta/+}$ EC, knockdown of SHIP2 reduced SHIP2 activity (**Fig. 7B**), and enhanced superoxide concentrations (**Fig. 7C**). We examined potential sources of superoxide, and again demonstrated increased Nox2 NADPH oxidase expression (**Fig. 7D**); moreover, the excess superoxide seen in SHIP2 deficient cells was inhibited by Gp91ds-tat (**Figs. 7E,F**). Furthermore, in SHIP2 knockdown HUVEC, S473 pAkt and S1177 peNOS were more abundant (**Fig. 7G**), and superoxide abundance was reduced by the PI3K inhibitors Wortmannin and LY294002 (**Fig. 7H**). These data imply increased PI3K signaling drives Nox2-dependent superoxide production in the context of human EC SHIP2 knockdown.

Discussion

We provide a number of novel findings pertaining to the understanding of endothelial SHIP2 signaling and metabolic disease: **1)** EC-specific reduction of SHIP2 activity is not associated with developmental defects; **2)** Mice with EC-specific reduction of SHIP2 activity develop insulin resistance in skeletal muscle and fat, which is not associated with evidence of inflammation; **3)** EC-specific reduction of SHIP2 activity is associated with endothelial dysfunction, excess superoxide abundance, and reduced NO bioavailability; **4)** Oxidative stress associated with SHIP2 knockdown in murine and human EC is caused by excessive PI3K signaling, and is Nox2 NADPH oxidase-dependent. Our data emphasize the detrimental impact of increased PI3K/Akt signaling on EC function, and confirm the key role of SHIP2 in maintaining vascular homeostasis. In particular, they reveal that increased basal PI3K/Akt signal transduction in EC is associated with Nox2-mediated vascular oxidative stress and paradoxical systemic insulin resistance due to impaired adipose tissue and skeletal muscle glucose uptake. Therefore, whilst hyperinsulinemia is an adaptive response to hyperglycemia, when sustained this may have detrimental effects on vascular function *and* glucose uptake in key metabolic tissues; this raises important questions about the long-term risks of therapies that induce sustained insulin signaling.

SHIP2, insulin signaling, PI3-kinase and Akt. The ligand-bound insulin receptor phosphorylates tyrosine residues on downstream substrates, activating PI3K, which catalyzes phosphorylation of the 3'-position of inositol rings, generating 3' phosphoinositides including $PI(3,4,5)P_3$ (21). $PI(3,4,5)P_3$ recruits the serine/threonine kinase Akt to the cell membrane, facilitating its activation, allowing phosphorylation of downstream effectors, including eNOS (19). Short-term *in vivo* studies have examined the effect of SHIP2 modulation on insulin sensitivity in models of type 2 diabetes. Adenoviral expression of a dominant-negative mutant

SHIP2 in the liver of obese hyperglycemic mice restored insulin sensitivity and Akt phosphorylation (22), whereas expression of wild-type SHIP2 blunted these (23). In humans, SHIP2 (*Inppl1*) polymorphisms are associated with obesity, type 2 diabetes and the metabolic syndrome (24,25). SHIP2 inhibition has thus been suggested as an approach to treat insulin resistant type 2 diabetes mellitus (7). However, the effect of SHIP2 inhibition on specific components of the arterial wall is ill defined; our data question the potential therapeutic benefit of SHIP2 inhibition, at least in the endothelium.

Endothelial SHIP2 inhibition and glucose homeostasis. We demonstrated that 10-month old ECSHIP2$^{\Delta/+}$ mice were resistant to insulin-mediated glucose lowering, and the vascular dysfunction caused by chronic SHIP2 inactivation may underpin these findings. We found reduced insulin-stimulated eNOS activation in ECSHIP2$^{\Delta/+}$ EC, and endothelial-derived NO is thought to be crucial for insulin-stimulated glucose uptake; eNOS deficient mice are systemically insulin resistant, with reduced insulin-mediated glucose uptake in skeletal muscle (26,27). Kubota *et al* demonstrated impaired insulin-stimulated glucose disposal in the skeletal muscle of mice with endothelium-specific deletion of insulin receptor substrate 2 (IRS2), due to impaired NO bioavailability (28). Our dataset are consistent with this, since ECSHIP2$^{\Delta/+}$ mice have reduced EC insulin sensitivity, diminished insulin-stimulated glucose uptake to skeletal muscle, and reduced endothelial NO generation. However, mice with endothelium-specific insulin receptor deletion have normal glucose disposal during clamping studies (29), suggesting a complex association between vascular insulin signaling and systemic glucose homeostasis. Importantly, ECSHIP2$^{\Delta/+}$ mice had preserved proximal insulin signaling, implying that downstream signaling may be more important in vascular homeostasis, including regulation of systemic glucose metabolism.

Endothelial SHIP2 inhibition, superoxide generation, and eNOS inhibition. We demonstrate that EC-specific inactivation of SHIP2 increases basal activation of the PI3K/Akt/eNOS signaling cascade, with potentially important increases in both the total and phosphorylated forms of key signaling nodes (which did not increase in response to insulin), and increases the abundance of superoxide. This is associated with reduced NO production in isolated EC, and aortic segments under isometric tension, indicating endothelial dysfunction. Expression of Nox2 NADPH oxidase was increased in the setting of SHIP2 knockdown, and by using the selective antagonist Gp91ds-tat, we implicated Nox2 as the source of excess superoxide. Moreover, by normalizing superoxide abundance using two selective PI3K inhibitors, we also implicated excessive PI3K/Akt signaling as contributing to oxidative stress. Whilst a number of studies have shown a link between excessive Akt activation and superoxide generation (30,31), none have identified the source of excess superoxide. Moreover, the association between SHIP2 and oxidative stress *in vivo* is currently unexplored. Our study is therefore the first to mechanistically link SHIP2 inactivation to increased Nox2 NADPH oxidase activity, oxidative stress, and endothelial dysfunction (**Fig. 8**). By recapitulating these data in human EC after silencing SHIP2, we provide support for the relevance of our *in vivo* observations to human pathophysiology, suggesting caution is warranted in the clinical translation of SHIP2 inhibition. Importantly, we have also published that mice with endothelial overexpression of the insulin receptor exhibit many of the phenotypic traits noted in ECSHIP2$^{\Delta/+}$ mice, including PI3K- and Nox2-dependent vascular oxidative stress and endothelial dysfunction (12). In conjunction, these data suggest that unrestrained signaling at multiple nodes in the proximal insulin signaling cascade cause vascular dysfunction mediated by Nox2-dependent oxidative stress.

Conclusion. Vascular endothelial SHIP2 activity is required to maintain normal systemic insulin sensitivity and suppress vascular oxidative stress and endothelial dysfunction caused by unrestrained PI3K-Nox2 signaling.

Author contributions

NTW collected data and wrote the manuscript; MCG collected data; PAP collected data and wrote the manuscript; HV collected data; PS collected data; SG collected data; NYY collected data; HI collected data; KJG collected data; NM collected data; AS collected data; KB collected data; DJB contributed to discussion and reviewed/edited manuscript; SS provided materials, contributed to discussion and reviewed/edited manuscript; SBW contributed to discussion and reviewed/edited manuscript; MTK wrote manuscript and acts as study guarantor; RMC collected data and wrote manuscript.

Acknowledgements

This work was supported by British Heart Foundation grant RG09/010. MTK is British Heart Foundation Professor of Cardiovascular and Diabetes research; SBW is supported by a European Research Council starter award 310747. RMC is supported by British Heart Foundation Intermediate research Fellowship FS/12/80/29821, DJB is Wellcome Trust Investigator. PAP and AMNW are supported by a British Heart Foundation Clinical Research Training Fellowships.

References

1. Johnson AMF, Olefsky JM. The Origins and Drivers of Insulin Resistance. Cell 2013; 152: 673–84.

2. Duncan ER, Walker SJ, Ezzat VA, Wheatcroft SB, Li JM, Shah AM, Kearney MT. Accelerated endothelial dysfunction in mild prediabetic insulin resistance: the early role of reactive oxygen species. Am J Physiol Endocrinol Metab 2007; 293:E1311–9.

3. Wheatcroft SB, Shah AM, Li J-M, Duncan E, Noronha BT, Crossey PA, Kearney MT. Preserved Glucoregulation but Attenuation of the Vascular Actions of Insulin in Mice Heterozygous for Knockout of the Insulin Receptor. Diabetes 2004; 53: 2645–52.

4. Sukumar P, Viswambharan H, Imrie H, Cubbon RM, Yuldasheva N, Gage M, Galloway S, Skromna A, Kandavelu P, Santos CX, Gatenby VK, Smith J, Beech DJ, Wheatcroft SB, Channon KM, Shah AM, Kearney MT. Nox2 NADPH Oxidase Has a Critical Role in Insulin Resistance–Related Endothelial Cell Dysfunction. Diabetes 2013; 62: 2130–4.

5. Duncan ER, Crossey PA, Walker S, Anilkumar N, Poston L, Douglas G, Ezzat VA, Wheatcroft SB, Shah AM, Kearney MT. Effect of Endothelium-Specific Insulin Resistance on Endothelial Function In Vivo. Diabetes 2008; 57: 3307–14.

6. Noronha BT, Li JM, Wheatcroft SB, Shah AM, Kearney MT. Inducible Nitric Oxide Synthase Has Divergent Effects on Vascular and Metabolic Function in Obesity. Diabetes 2005; 54: 1082–9.

7. Lazar DF, Saltiel AR. Lipid phosphatases as drug discovery targets for type 2 diabetes. Nat Rev Drug Discov 2006; 5: 333–42.

8. Kagawa S, Soeda Y, Ishihara H, Oya T, Sasahara M, Yaguchi S, Oshita R, Wada T, Tsuneki H, Sasaoka T. Impact of Transgenic Overexpression of SH2-Containing Inositol 5′-Phosphatase 2 on Glucose Metabolism and Insulin Signaling in Mice. Endocrinology 2008; 149: 642–50.

9. Clement S, Krause U, Desmedt F, Tanti J-F, Behrends J, Pesesse X, Sasaki T, Penninger J, Doherty M, Malaisse W, Dumont JE, Le Marchand-Brustel Y, Erneux C. Hue L, Schurmans S. The lipid phosphatase SHIP2 controls insulin sensitivity. Nature 2001; 409: 92–7.

10. Sleeman MW, Wortley KE, Lai K-M V, Gowen LC, Kintner J, Kline WO, Garcia K, Stitt TN, Yancopoulos GD, Wiegand SJ, Glass DJ. Absence of the lipid phosphatase SHIP2 confers resistance to dietary obesity. Nat Med 2005; 11: 199–205.

11. Dubois E, Jacoby M, Blockmans M, Pernot E, Schiffmann SN, Foukas LC, Henquin JC, Vanhaesebroeck B, Erneux C, Schurmans S. Developmental defects and rescue from glucose intolerance of a catalytically-inactive novel Ship2 mutant mouse. Cell Signal 2012; 24: 1971–80.

12. Viswambharan H, Yuldasheva NY, Sengupta A, Imrie H, Gage MC, Haywood NJ, Walker AM, Skromna A, Makova N, Galloway SL, Shah P, Sukumar P, Porter KE, Grant PJ, Shah AM, Santos CX, Li J, Beech DJ, Wheatcroft S, Cubbon RM, Kearney MT. Selective Enhancement of Insulin Sensitivity in the Endothelium In Vivo Reveals a Novel Proatherosclerotic Signalling Loop. Circ Res 2017; 120: 784–98.

13. Anderson EJ, Lustig ME, Boyle KE, Woodlief TL, Kane DA, Lin CT, Price JW 3rd, Kang L, Rabinovitch PS, Szeto HH, Houmard JA, Cortright RN, Wasserman DH, Neufer PD. Mitochondrial H2O2 emission and cellular redox state link excess fat intake to insulin resistance in both rodents and humans. J Clin Invest 2009; 119: 573–81.

14. Abbas A, Imrie H, Viswambharan H, Sukumar P, Rajwani A, Cubbon RM, Gage M, Smith J, Galloway S, Yuldeshava N, Kahn M, Xuan S, Grant PJ, Channon KM, Beech DJ, Wheatcroft SB, Kearney MT. The Insulin-Like Growth Factor-1 Receptor Is a Negative Regulator of Nitric Oxide Bioavailability and Insulin Sensitivity in the Endothelium. Diabetes 2011; 60: 2169–78.

15. Imrie H, Viswambharan H, Sukumar P, Abbas A, Cubbon RM, Yuldasheva N, Gage M, Smith J, Galloway S, Skromna A, Rashid ST, Futers TS, Xuan S, Gatenby VK, Grant PJ, Channon KM, Beech DJ, Wheatcroft SB, Kearney MT. Novel Role of the IGF-1 Receptor in Endothelial Function and Repair. Diabetes 2012; 61: 2359–68.

16. Li J, Hou B, Tumova S, Muraki K, Bruns A, Ludlow MJ, Sedo A, Hyman AJ, McKeown L, Young RS, Yuldasheva NY, Majeed Y, Wilson LA, Rode B, Bailey MA, Kim HR, Fu Z, Carter DA, Bilton J, Imrie H, Ajuh P, Dear TN, Cubbon RM, Kearney MT, Prasad KR, Evans PC, Ainscough JF, Beech DJ. Piezo1 integration of vascular architecture with physiological force. Nature 2014; 515: 279–82.

17. Cubbon R, Yuldasheva N, Viswambharan H, Mercer B, Baliga V, Stephen SL, Askham J, Sukumar P, Skromna A, Mughal RS, Walker AM, Bruns A, Bailey MA, Galloway S, Imrie H, Gage MC, Rakobowchuk M, Li J, Porter KE, Ponnambalam S, Wheatcroft SB, Beech DJ, Kearney MT. Restoring Akt1 activity in outgrowth endothelial cells from South Asian men rescues vascular reparative potential. Stem Cells 2014; 32: 2714–23.

18. Dalmas E, Toubal A, Alzaid F, Blazek K, Eames HL, Lebozec K, Pini M, Hainault I, Montastier E, Denis RG, Ancel P, Lacombe A, Ling Y, Allatif O, Cruciani-Guglielmacci C, André S, Viguerie N, Poitou C, Stich V, Torcivia A, Foufelle F, Luquet S, Aron-Wisnewsky J, Langin D, Clément K, Udalova IA, Venteclef N. Irf5 deficiency in macrophages promotes beneficial adipose tissue expansion and insulin sensitivity during obesity. Nat Med 2015; 21: 610–8.

19. Engelman JA, Luo J, Cantley LC. The evolution of phosphatidylinositol 3-kinases as regulators of growth and metabolism. Nat Rev Genet 200; 7: 606–19.

20. Manning BD, Cantley LC. AKT/PKB Signaling: Navigating Downstream. Cell 2007; 129: 1261–74.

21. Taniguchi CM, Emanuelli B, Kahn CR. Critical nodes in signalling pathways: insights

into insulin action. Nat Rev Mol Cell Biol 2006; 7: 85–96.

22. Grempler R, Zibrova D, Schoelch C, van Marle A, Rippmann JF, Redemann N. Normalization of Prandial Blood Glucose and Improvement of Glucose Tolerance by Liver-Specific Inhibition of SH2 Domain–Containing Inositol Phosphatase 2 (SHIP2) in Diabetic KKAy Mice. Diabetes 2007; 56: 2235–41.

23. Fukui K, Wada T, Kagawa S, Nagira K, Ikubo M, Ishihara H, Kobayashi M, Sasaoka T. Impact of the Liver-Specific Expression of SHIP2 (SH2-Containing Inositol 5′-Phosphatase 2) on Insulin Signaling and Glucose Metabolism in Mice. Diabetes 2005; 54: 1958–67.

24. Marion E, Kaisaki PJ, Pouillon V, Gueydan C, Levy JC, Bodson A, Krzentowski G, Daubresse JC, Mockel J, Behrends J, Servais G, Szpirer C, Kruys V, Gauguier D, Schurmans S. The Gene INPPL1, Encoding the Lipid Phosphatase SHIP2, Is a Candidate for Type 2 Diabetes In Rat and Man. Diabetes 2002; 51: 2012–7.

25. Kaisaki PJ, Delépine M, Woon PY, Sebag-Montefiore L, Wilder SP, Menzel S, Vionnet N, Marion E, Riveline JP, Charpentier G, Schurmans S, Levy JC, Lathrop M, Farrall M, Gauguier D. Polymorphisms in Type II SH2 Domain–Containing Inositol 5-Phosphatase (INPPL1, SHIP2) Are Associated With Physiological Abnormalities of the Metabolic Syndrome. Diabetes 2004; 53: 1900–4.

26. Duplain H, Burcelin R, Sartori C, Cook S, Egli M, Lepori M, Vollenweider P, Pedrazzini T, Nicod P, Thorens B, Scherrer U. Insulin Resistance, Hyperlipidemia, and Hypertension in Mice Lacking Endothelial Nitric Oxide Synthase. Circulation 2001; 104: 342–5.

27. Shankar RR, Wu Y, Shen HQ, Zhu JS, Baron AD. Mice with gene disruption of both endothelial and neuronal nitric oxide synthase exhibit insulin resistance. Diabetes 2000; 49: 684–7.

28. Kubota T, Kubota N, Kumagai H, Yamaguchi S, Kozono H, Takahashi T, Inoue M, Itoh S, Takamoto I, Sasako T, Kumagai K, Kawai T, Hashimoto S, Kobayashi T, Sato M, Tokuyama K, Nishimura S, Tsunoda M, Ide T, Murakami K, Yamazaki T, Ezaki O, Kawamura K, Masuda H, Moroi M, Sugi K, Oike Y, Shimokawa H, Yanagihara N, Tsutsui M, Terauchi Y, Tobe K, Nagai R, Kamata K, Inoue K, Kodama T, Ueki K, Kadowaki T. Impaired Insulin Signaling in Endothelial Cells Reduces Insulin-Induced Glucose Uptake by Skeletal Muscle. Cell Metab 2011; 13: 294–307.

29. Vicent D, Ilany J, Kondo T, Naruse K, Fisher SJ, Kisanuki YY, Bursell S, Yanagisawa M, King GL, Kahn CR. The role of endothelial insulin signaling in the regulation of vascular tone and insulin resistance. J Clin Invest 2003; 111: 1373–80.

30. Wang C-Y, Kim H-H, Hiroi Y, Sawada N, Salomone S, Benjamin LE, Walsh K, Moskowitz MA, Liao JK. Obesity Increases Vascular Senescence and Susceptibility to Ischemic Injury Through Chronic Activation of Akt and mTOR. Sci Signal 2009; 2: ra11.

31. Kerr BA, Ma L, West XZ, Ding L, Malinin NL, Weber ME, Tischenko M, Goc A, Somanath PR, Penn MS, Podrez EA, Byzova TV. Interference with Akt Signaling Protects Against Myocardial Infarction and Death by Limiting the Consequences of Oxidative Stress. Sci Signal 2013; 6: ra67.

Figure Legends

Figure 1: Basic characterization of mice with endothelial cell specific inactivation of Shc homology 2-containing inositol 5´ phosphatase 2 (ECSHIP2$^{\Delta/+}$). Compared to control Cre^{+} littermate controls: **A)** No difference was seen in gross development of ECSHIP2$^{\Delta/+}$; **B)** ECSHIP2$^{\Delta/+}$ organ weights were comparable (n≥7); **C)** Nose to tail length of ECSHIP2$^{\Delta/+}$ was similar (n≥4); **D)** ECSHIP2$^{\Delta/+}$ were slightly heavier (n≥6); **E)** Truncated SHIP2 mRNA was detectable in organs from ECSHIP2$^{\Delta/+}$, but not controls (n=3); **F)** Truncated SHIP2 mRNA was only detectable in EC from ECSHIP2$^{\Delta/+}$ lungs, and not the non-EC fraction (n=3); **G)** SHIP2 protein expression (Representative Western blot shown above panel) was mildly reduced in EC from ECSHIP2$^{\Delta/+}$ (n≥5); **I)** SHIP2 activity was substantially reduced in EC from ECSHIP2$^{\Delta/+}$ (n≥9).

Figure 2. Abnormal glucose homeostasis in ECSHIP2$^{\Delta/+}$ mice. A) Fasting glucose was increased in ECSHIP2$^{\Delta/+}$ (n=7). **B)** Fasting insulin was comparable to control in ECSHIP2$^{\Delta/+}$ (n≥6). **C)** HOMA-IR was increased in ECSHIP2$^{\Delta/+}$ (n≥12). **D)** Glucose tolerance was impaired in ECSHIP2$^{\Delta/+}$ (n≥8). **E)** Insulin tolerance testing was similar in ECSHIP2$^{\Delta/+}$ versus control (n≥8). **F**) Serum free fatty acids were similar in ECSHIP2$^{\Delta/+}$ versus control (n≥6). **G**) Serum triglycerides were similar in ECSHIP2$^{\Delta/+}$ versus control (n≥6).

Figure 3. Insulin resistance in ECSHIP2$^{\Delta/+}$ during hyperinsulinemic euglycemic clamping. A) Reduced insulin infusion rate (GIR) in ECSHIP2$^{\Delta/+}$ indicative of insulin resistance. **B)** Blunted glucose uptake in muscle and fat from ECSHIP2$^{\Delta/+}$. **C,D)** Comparable hepatic glucose output in ECSHIP2$^{\Delta/+}$ versus control (n≥4 for all experiments).

Figure 4. Endothelial cell signaling insulin and mechanical shear stress signaling is impaired in ECSHIP2$^{\Delta/+}$. A) The basal abundance of Akt, pAkt T308, PDK1, pPDK1,

Rictor, pRictor, eNOS and peNOS S1177 were increased in ECSHIP2$^{\Delta/+}$ EC exposed to standard culture media (n≥4). **B)** Insulin-stimulated [150nm for 10 minutes] phosphorylation of eNOS, but not Akt, was impaired in ECSHIP2$^{\Delta/+}$ EC (n≥6). **C)** Shear stress-induction [10 minutes] of Akt and eNOS phosphorylation was impaired in ECSHIP2$^{\Delta/+}$ EC (n≥6). Representative Western blots are shown above all panels.

Figure 5. Impaired aortic vasodilation in ECSHIP2$^{\Delta/+}$ is associated with oxidative stress and reduced NO bioavailability. A) Reduced insulin mediated aortic relaxation in ECSHIP2$^{\Delta/+}$ (n≥4). **B-D)** Reduced L-NMMA induced vasoconstriction in ECSHIP2$^{\Delta/+}$ indicative of reduced NO bioavailability (n≥3). **E,F)** Subtle impairment of acetylcholine-mediated vasodilation in aorta from ECSHIP2$^{\Delta/+}$ (n≥8). **F)** No difference in SNP-mediated vasodilatation in aortic rings from ECSHIP2$^{\Delta/+}$ (n≥3). **G-K)** MnTmPYP blunts acetylcholine-mediated vasodilation in aorta from ECSHIP2$^{\Delta/+}$ and controls, but the reduction in acetylcholine-mediated vasodilation is greater in ECSHIP2$^{\Delta/+}$ (n≥4). **L**) Increased aortic hydrogen peroxide generation in ECSHIP2$^{\Delta/+}$ (n≥4).

Figure 6. ECSHIP2$^{\Delta/+}$ endothelial cells exhibit PI3K- and Nox2-dependent oxidative stress, and reduced nitric oxide generation. A) Increased superoxide generation in ECSHIP2$^{\Delta/+}$, measured with lucigenin-enhanced chemiluminescence (left: n≥10) and DHE fluorescence (right: n≥3). **B)** Increased Nox2 NADPH oxidase protein (Representative Western blot shown above panel) in ECSHIP2$^{\Delta/+}$ (n≥9). **C)** Increased superoxide abundance in ECSHIP2$^{\Delta/+}$ is normalized by Gp91ds-tat (n≥4). **D)** Increased superoxide abundance in ECSHIP2$^{\Delta/+}$ is normalized by the PI3K inhibitors Wortmannin and LY294002 (n≥4). **E)** Insulin-stimulated NO production is impaired in endothelial cells from ECSHIP2$^{\Delta/+}$ (n≥5).

Figure 7. shRNA knockdown of SHIP2 in human umbilical vein endothelial cells (HUVEC) recapitulates phenotype of ECSHIP2$^{\Delta/+}$ endothelial cells. A) SHIP2 shRNA reduced SHIP2 protein by approximately 75%, versus control shRNA (n=3; Representative Western blot shown above panel). **B)** SHIP2 activity is reduced by SHIP2 shRNA (n=3). **C)** Increased superoxide abundance in SHIP2 knockdown HUVEC measured by lucigenin-enhanced chemiluminescence (n=3). **D)** Increased Nox2 NADPH oxidase protein in SHIP2 knockdown HUVEC (n=5; Representative Western blot shown above panel). **E,F)** Suppression of excess superoxide production in SHIP2 knockdown HUVEC by the NOX2 inhibitor Gp91ds-tat, measured with lucigenin-enhanced chemiluminescence (**E**) ($n \geq 3$) and DHE fluorescence (**F**) (n=6). **G)** Increased concentration of S473 pAkt, S1177 peNOS in SHIP2 knockdown HUVEC (n=5). **H)** Suppression of excess superoxide production in SHIP2 knockdown HUVEC by the PI3K inhibitors Wortmannin and LY294002 (n=5).

Figure 8. Proposed mechanism of endothelial dysfunction associated with SHIP2 knockdown. In contract with normal physiology (A), reduced SHIP2 activity (B) results in increased basal PI3K/Akt/eNOS signaling, although NOX2 is also hyper-activated, resulting in oxidative stress and reduced nitric oxide bioavailability.

Figure 1

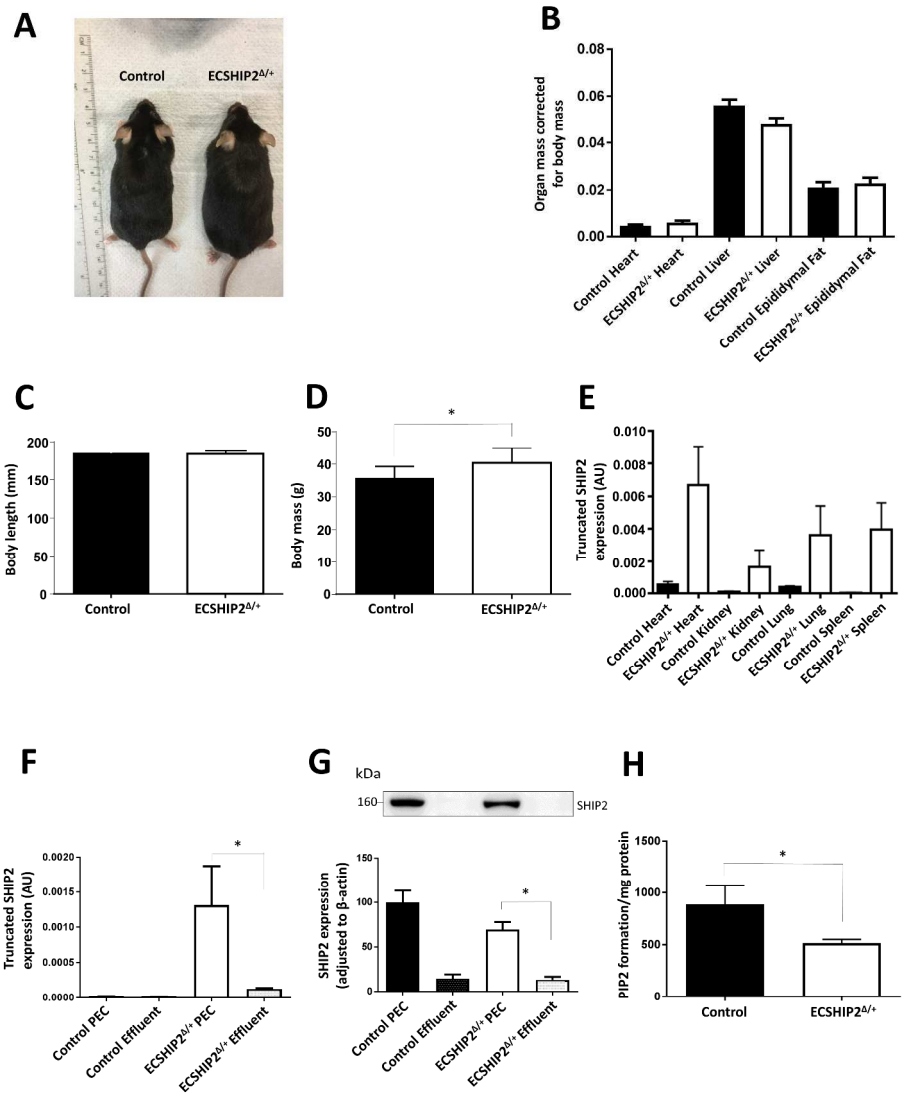

Figure 1

952x1270mm (96 x 96 DPI)

Figure 2

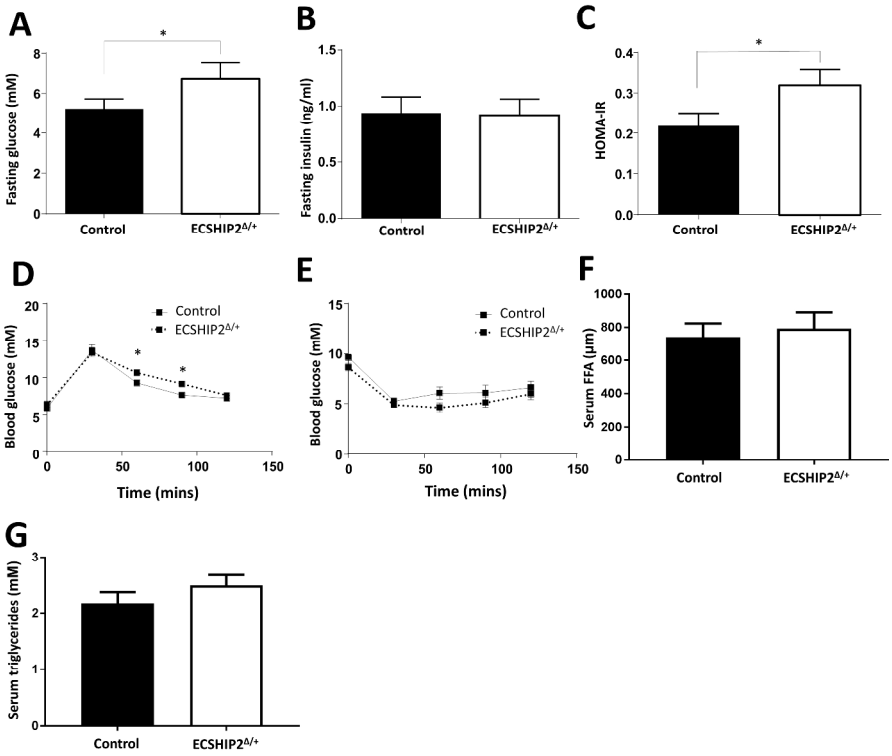

Figure 2

952x1270mm (96 x 96 DPI)

Figure 3

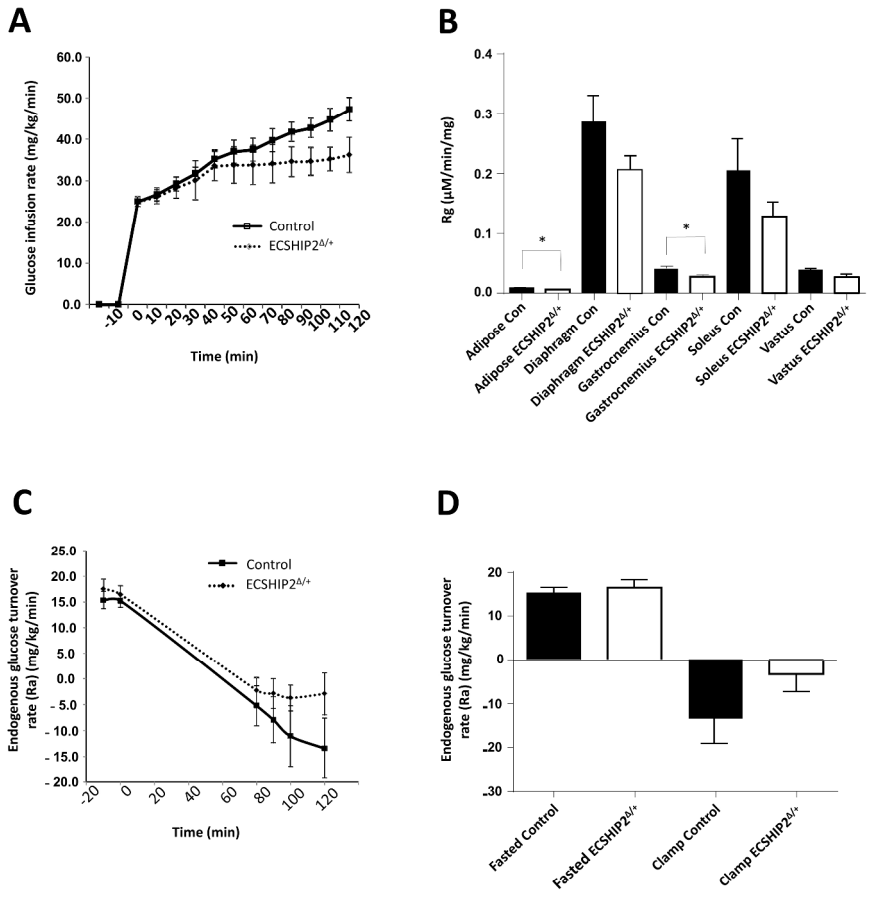

Figure 3

952x1270mm (96 x 96 DPI)

Figure 4

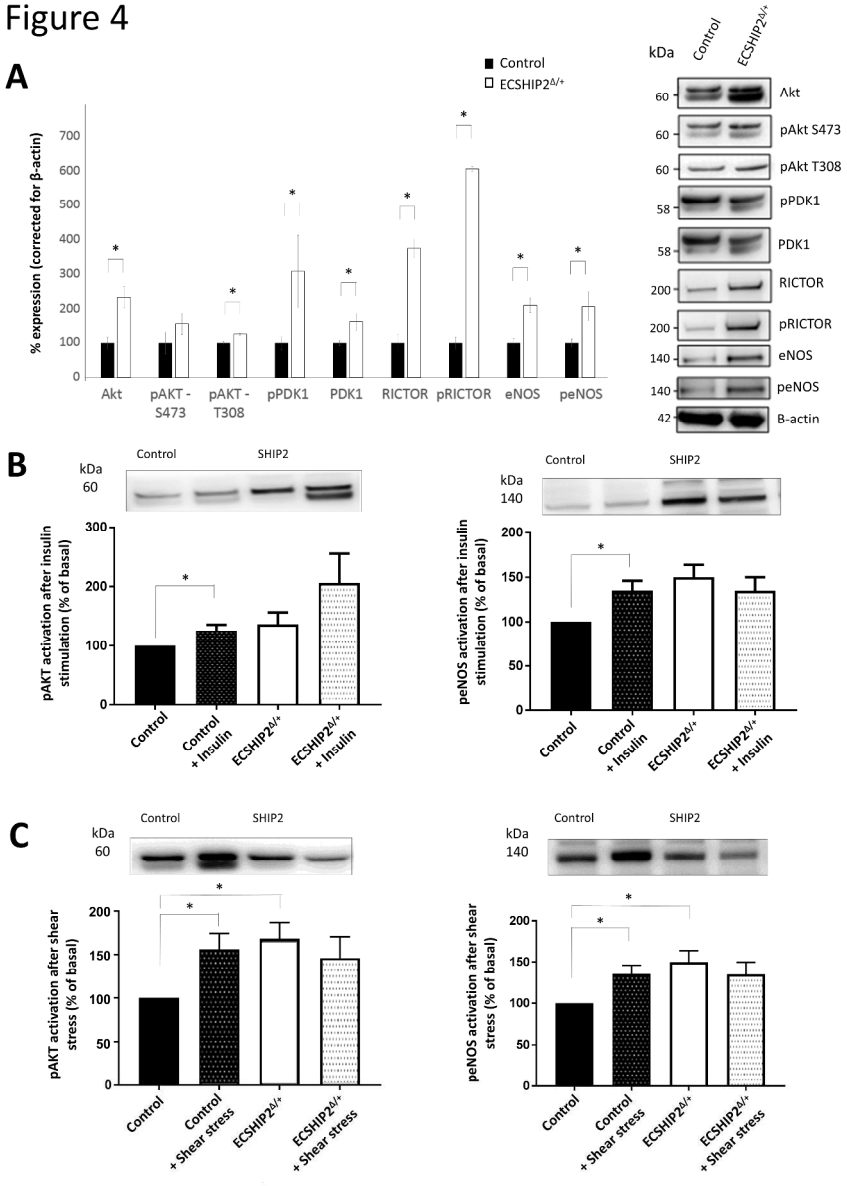

Figure 4

952x1270mm (96 x 96 DPI)

Figure 5

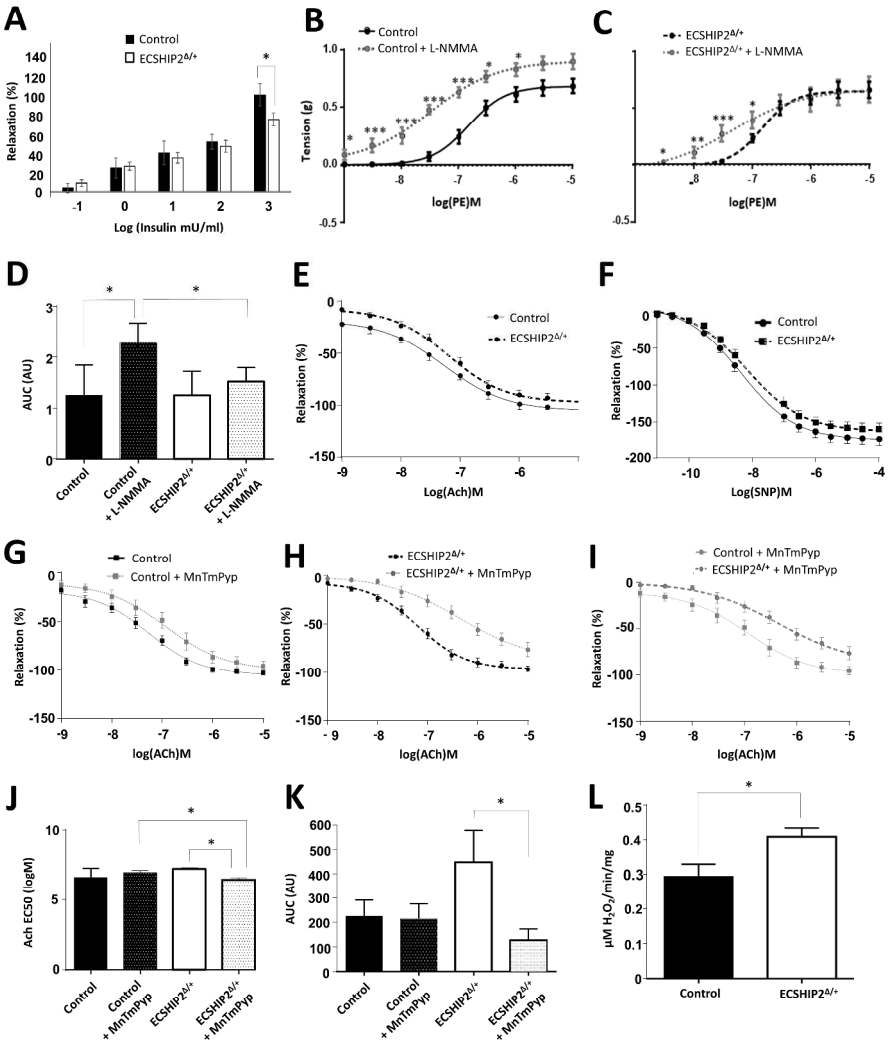

Figure 5

952x1270mm (96 x 96 DPI)

Figure 6

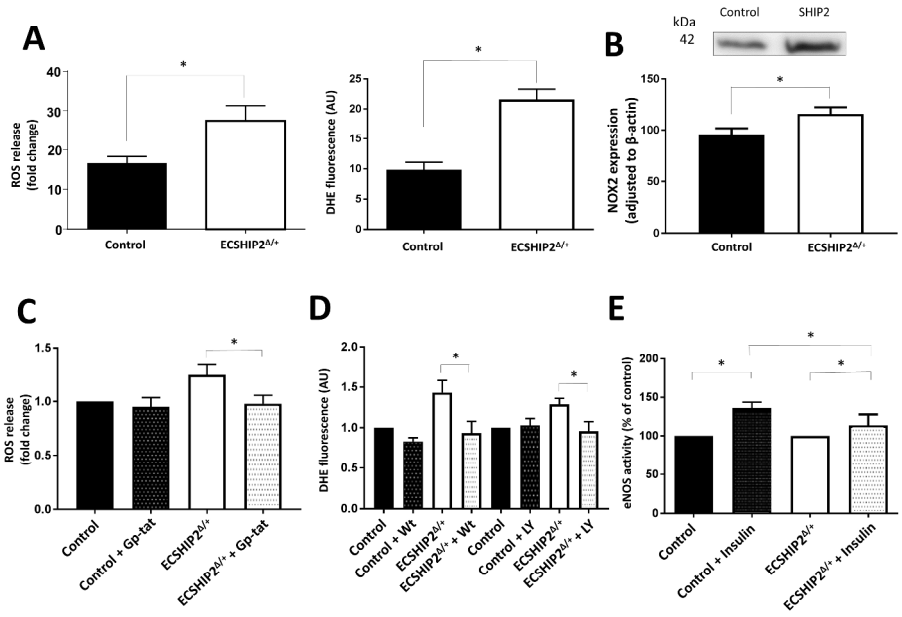

Figure 6

952x1270mm (96 x 96 DPI)

Figure 7

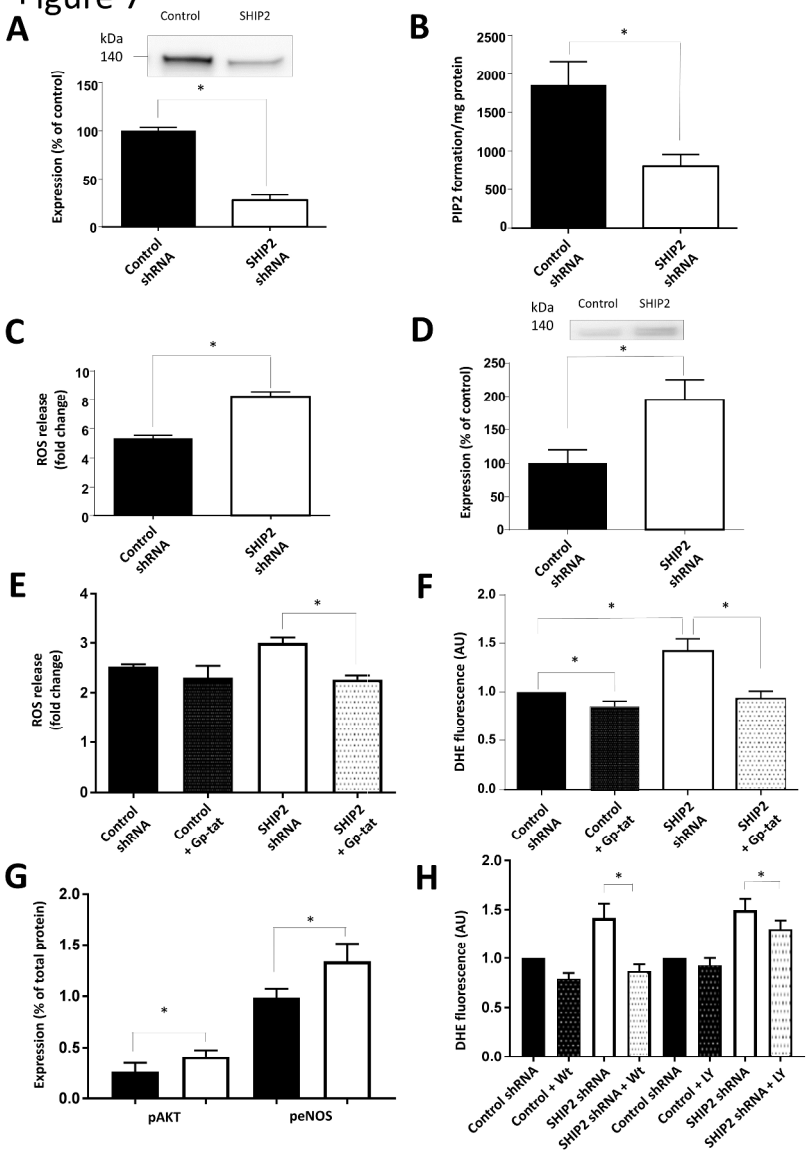

Figure 7

952x1270mm (96 x 96 DPI)

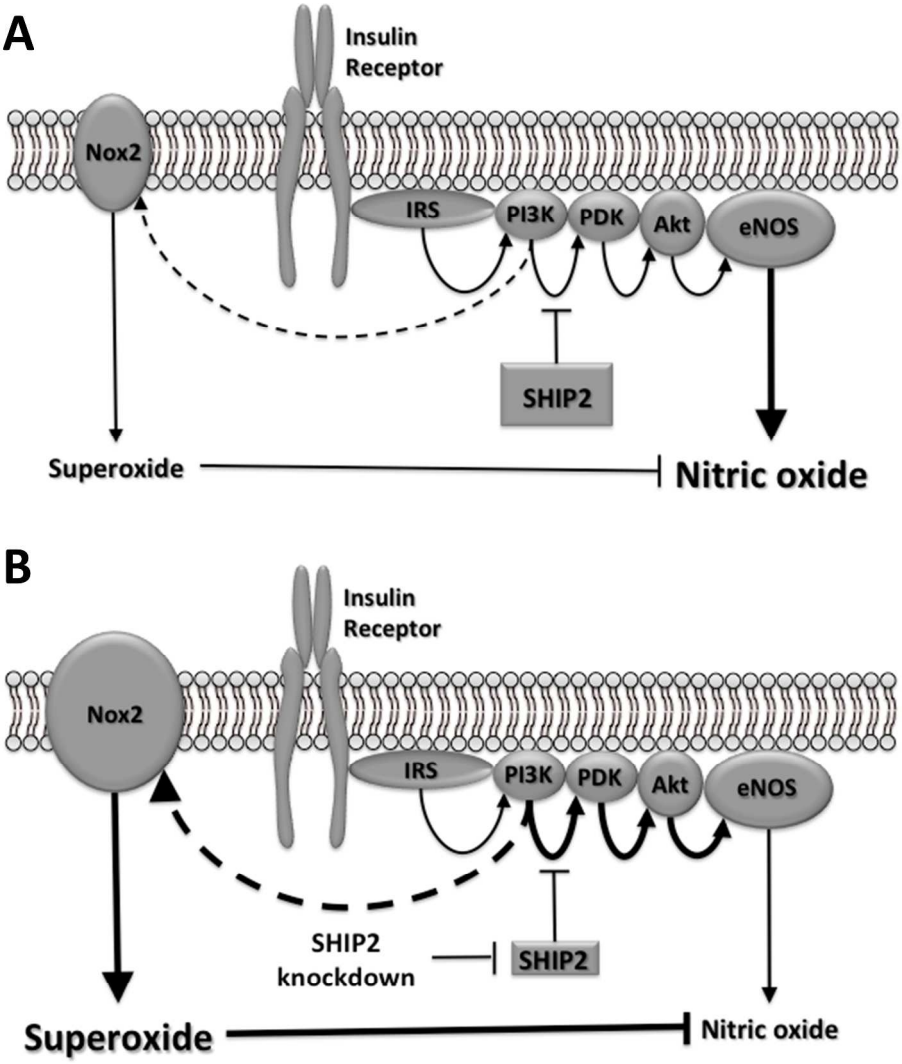

Figure 8

952x1270mm (96 x 96 DPI)

Online supplemental materials

Supplemental Figure Legends

Supplemental Figure 1: ECSHIP2$^{\Delta/+}$ mice do not exhibit a pro-inflammatory state. A) Truncated SHIP2 mRNA was detectable in CD11b^{+} myeloid cells from ECSHIP2$^{\Delta/+}$, although >3000-fold lower level than in lung EC (n=4,4,2). **B)** Blood leukocyte populations were comparable in ECSHIP2$^{\Delta/+}$ and control littermates (n≥8). **C)** Peripheral blood mononuclear cell SHIP2 activity was not altered in ECSHIP2$^{\Delta/+}$ (n=6,7). **D,E)** Serum TNFα and IL-6 were comparable in ECSHIP2$^{\Delta/+}$ and control littermates (n=8,14). **F)** ECSHIP2$^{\Delta/+}$ had similar TNFα, IL-6, and IL-1β mRNA expression in white adipose tissue and skeletal muscle (n≥4). **G)** White adipose tissue collagen staining with Sirius Red, a feature of chronic inflammation, was similar in ECSHIP2$^{\Delta/+}$ and control littermates (n=6,11).

Supplemental Figure 2: Juvenile ECSHIP2$^{\Delta/+}$ mice have normal EC expression of key signaling nodes and vascularization of metabolic tissues. A) The increased expression of Akt, Rictor and eNOS seen in 10-month old ECSHIP2$^{\Delta/+}$ mice was not apparent in 6-week old mice (n≥5). **B,C)** 6-week old ECSHIP2$^{\Delta/+}$ mice exhibited normal capillary density in white adipose tissue and skeletal muscle (n=5,4).

Supplemental Figure 3: Insulin receptor and insulin receptor substrate 1/2 signaling is unchanged in ECSHIP2$^{\Delta/+}$ mice. A) Basal expression and phosphorylation of the insulin receptor and insulin receptor substrate 1/2 were comparable in ECSHIP2$^{\Delta/+}$ mice and littermate controls (n≥5). **B)** Insulin-stimulated phosphorylation of the insulin receptor and insulin receptor substrate 1/2 were comparable in ECSHIP2$^{\Delta/+}$ mice and littermate controls (n≥5).

Supplementary Figure 1

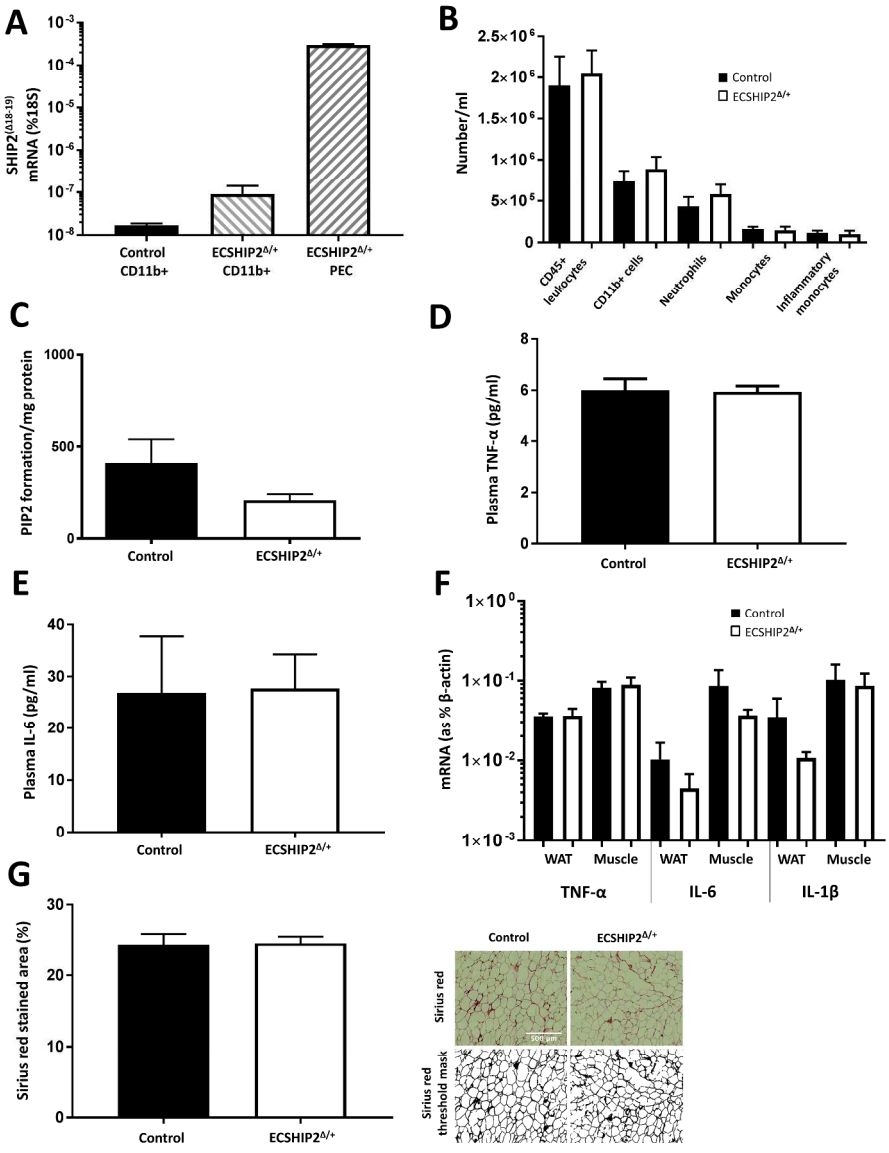

952x1270mm (96 x 96 DPI)

Supplementary Figure 2

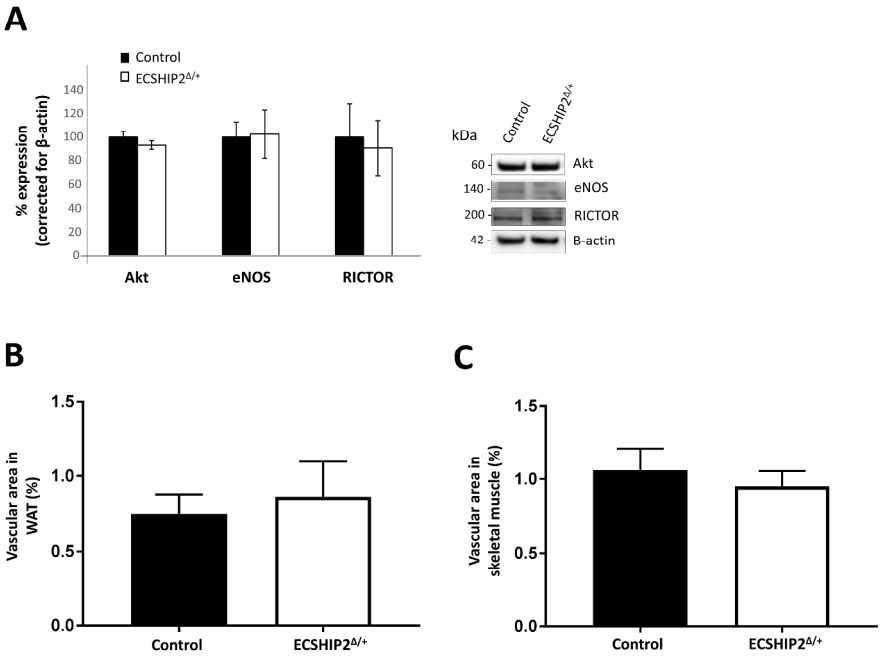

952x1270mm (96 x 96 DPI)

Supplementary Figure 3

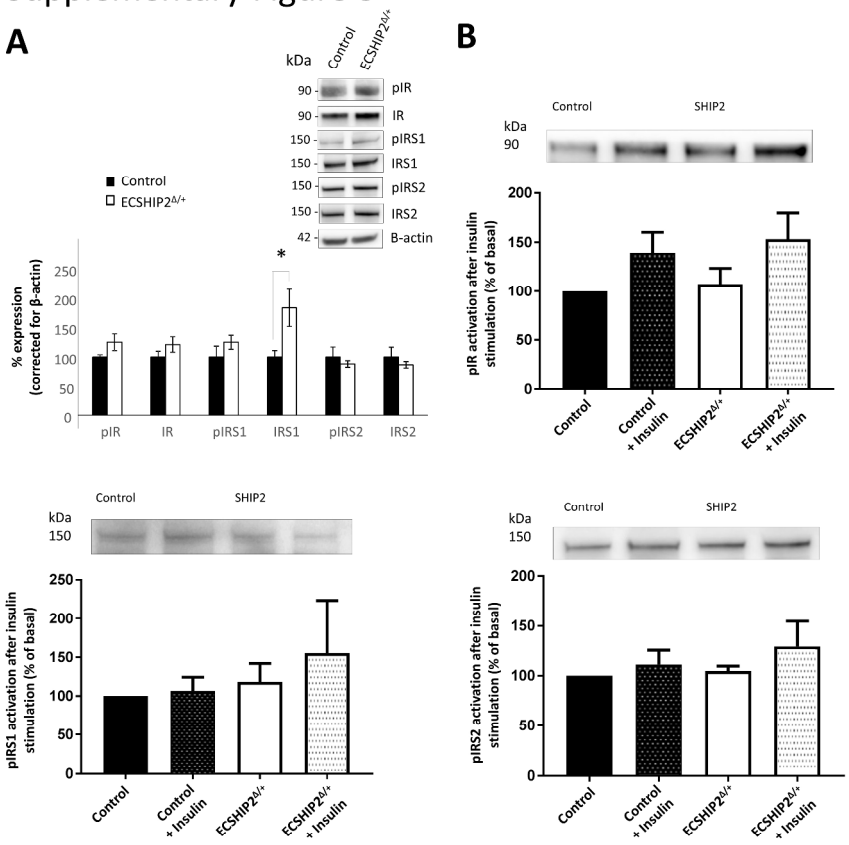

952x1270mm (96 x 96 DPI)